

# AC Impedance Spectroscopy Analysis of the Corrosion Behavior of Reinforced Concrete in Chloride Solution

Jinping Chen\* and Xuesong Zhang

College of Pipeline and Civil Engineering, China University of Petroleum, Qingdao, 266580, China

\*E-mail: [chenjp@upc.edu.cn](mailto:chenjp@upc.edu.cn)

*Received: 25 February 2017 / Accepted: 9 April 2017 / Published: 12 May 2017*

---

The degradation of a reinforced concrete structure will occur with corrosion activation, which is caused by the steel rebar depassivation as a result of chloride penetration into the structure. Herein, the reinforced concrete corrosion process in a chloride solution was analyzed using AC impedance spectroscopy. The activation of the corrosion is associated with a significant impedance response decline in the capacitive part, as highlighted through multielementary analyses, SEM observations and the low-frequency region of impedance spectra.

---

**Keywords:** Impedance spectroscopy; Corrosion; Reinforced concrete; Chloride

## 1. INTRODUCTION

Being potentially the most popular cause of the degradation of reinforced concrete, the reinforcing steel corrosion has been a focus of attention. As the interstitial solution in the concrete is highly alkaline, it provides natural corrosion prevention for the reinforcing steel [1]. However, the acidification of the environment in the vicinity of the rebars (i.e., carbonation) could suppress the passive state. An increase in the corrosive attack can also be achieved as sulfates, chlorides and other aggressive ions destroy the passive film. The penetration of chloride into reinforced concrete naturally leads to the reinforcing steel corrosion. The process of the rebar corrosion over the whole working life of a concrete structure includes phases of incubation and propagation [2]. The chloride penetrates into the porous material and accumulates near the steel in the former period, where the necessary chloride concentration for the corrosion initiation and the concrete layer determine the duration of this period. On the other hand, the depassivation of the surface of the reinforcing steel occurs in the latter period, where the corrosion develops and finally leads to the structure's destruction [3-10].

For its ability to show the concrete microstructure in the high-frequency region (above kilohertz), AC electrochemical impedance spectroscopy (EIS) has been recognized as an excellent non-destructive approach in the last several years [11-18]. The dispersive capacitance of the micro-pore system in the concrete, together with the concrete bulk resistance, explains the high-frequency EIS spectra of the capacitive loop in the Nyquist diagram. Usually, there is a similarity between the facile parallel linked capacitance  $C_1$  & resistance  $R_1$  equivalent circuit and this loop [19-24]. The quantification of the incubation period by the impedance technique and the investigation of the chloride's depassivation effect on a steel rebar (built into a cement-based material) are reported in this study. In addition, the determination of the threshold value for corrosion activation, representing a critical chloride concentration on the surface of the reinforcing steel, is demonstrated through a primary accelerated monitoring process proposed for reinforcing steel/cement-based material corrosion. The use of a constant electric field (for the chloride ion shift acceleration in cement-based materials) together with a non-destructive electrochemical method (EIS) serves as the basis for this process.

## 2. EXPERIMENTS

The sample adopted in this study was R235 reinforcing steel, whose composition in mass percentage is as follows: P<0.045; S<0.05; Si: 0.12–0.30; C: 0.14–0.22; Mn: 0.30–0.65; Fe: the balance. A cement-based material covered one face of the steel that was previously processed through sandblasting and rinsed by deionized water. Information on the conservation, manufacture and composition of this material is shown below. The chloride shift was restricted to one dimension through the application of a polyurethane resin on the electrically connected opposite face and the side faces at the reinforcing steel/cement-based material interface. Aggregate gradation, which complies with ASTM C33, was used, as well as ordinary Portland cement (Type I), which complies with ASTM C114.

**Table 1.** Mixture proportions of concrete and mechanical properties.

|   |  |                                       |     |
|---|--|---------------------------------------|-----|
| Cement ( $\text{kg/m}^3$ )                                  | 300  | Silica fume ( $\text{kg/m}^3$ )       | 121 |
| Water ( $\text{kg/m}^3$ )                                   | 210 (sample denoted as C-1)<br>150 (sample denoted as C-2)<br>60 (sample denoted as C-3) | Air content (%)                       | 1   |
| Fine aggregate ( $\text{kg/m}^3$ ) – fineness modulus = 2.8 | 650  | Compressive strength (MPa) at 28 days | 32  |
| Coarse aggregate ( $\text{kg/m}^3$ ) – max. size 20 mm      | 1200   |                                       |     |

Table 1 exhibits the traits of fresh and hardened concrete, in addition to the concrete mixture proportions. A piece of steel was cast through the center of an o in cylindrical samples. 24 h after the samples were constructed, they were demolded and cured for 28 days in an alkaline solution to decrease leaching and guarantee the saturation of the samples. Note that the solution simulates the cement-based material pore solution and bears a significant similarity to the test solution. This work prepared three diverse specimens (A, B and C) with various water/cement ratios.

Drying was conducted in an oven for the prismatic concrete samples. The specimens were subjected to 1%, chloride solution by weight. Before starting each measurement, the cell was assembled using the saturated calomel electrode (SCE, Hg/Hg<sub>2</sub>SO<sub>4</sub> sat K<sub>2</sub>SO<sub>4</sub>) as a reference, and the counter electrode (carbon) was placed on the concrete surface, providing a wet sponge to assure a good electrolytic contact, with the rebars serving as the working electrodes. The corrosion was monitored with ZPlot/CorrWare software installed on a computer and Solartron impedance analyzers, and a Solartron potentiostat and galvanostat were applied for the EIS measurements with a current range of 1 mA to 100 nA at 20 °C. 50 kHz and 10 mHz are the initial and final frequencies of the impedance scan, respectively, and 5 mV is its amplitude (rms). The specimen surfaces were observed using a JEOL 5410 LV scanning electron microscope after the corrosion test. In association with the SEM observation, an energy-dispersive X-ray (EDX) analysis and multielementary cartography were performed to characterize the corrosion products. Potentiometric titration tests with silver nitrate were performed in the downstream compartment after the NaCl addition. The measurement of the ionic flux in the steady state allows one to deduce the diffusion coefficient  $D_{ss}$ ,

$$D_{ss} = \frac{RT}{Z_{Cl} - F U} \frac{L}{\Delta t A C_0} \frac{\Delta C V_a}{\Delta t A C_0} \left(1 - e^{-\frac{zF}{RT} U}\right)$$

where  $V_a$  is the downstream compartment volume (m<sup>3</sup>),  $A$  is the cross-section area (m<sup>2</sup>),  $\Delta C$  is the variation of chloride concentration in the downstream compartment during a time range  $\Delta t$  (mol/m<sup>3</sup>),  $L$  is the specimen's thickness (m),  $C_0$  is the chloride concentration in the upstream cell (500 mol/m<sup>3</sup>),  $R$  is the gas constant (J/mol K),  $T$  is the reference temperature (K),  $z_{Cl^-}$  is the chloride ion valence,  $F$  is the Faraday constant (J/V mol) and  $U$  is the difference of potential (V).

### 3. RESULTS AND DISCUSSION

Being electrically fitted, an equivalent circuit is normally employed for the interpretation of the AC impedance spectra. It is generally accepted that a physical model of the steel/concrete interface consists of a layer of iron oxides and hydroxides in the form of a film in the passive stage and an interfacial film adjoined to the concrete matrix [25, 26]. The most favorable model is selected among its counterparts and is used for the corrosion current calculation since the reinforced concrete network is complicated [27-29]. An interfacial film adjacent to the concrete matrix and a passive film with a layer of hydroxides and iron oxides are universally recognized to make up a physical model of the steel/concrete interface [30]. Myriads of equivalent circuits have been suggested for describing the active and passive corrosion processes with macro-cell corrosion, passive film formation and diffusion control [31]. The equivalent electrical circuit range of the steel/concrete interface associated

impedances and the electrolyte resistance  $R_s$  in the pores of the concrete make up the steel/concrete interface, as shown in Figure 1. The steel reacts with the cement in the vicinity of the surface of steel, with the resulting products characterized by the impedance  $Z_1$ .

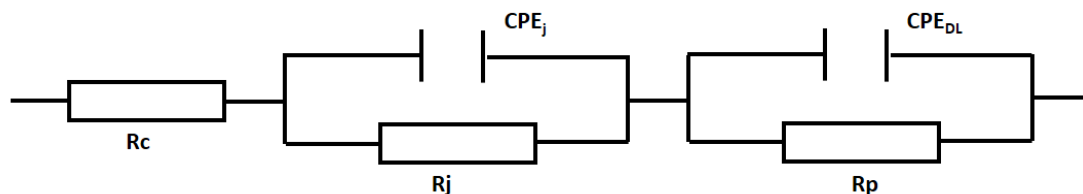


**Figure 1.** Equivalent circuit model for impedance simulation.

The corrosion products are generated on the surface of the metal and shape a film, the ionic resistance of which is denoted by the resistance  $R_f$ . The capacitance  $C_f$  and resistance  $R_f$  make up this impedance. The surface reaction, double-layer capacitance  $C_{dl}$  and diffusion impedance  $W$  are associated with the resistance  $R_{ct}$  at the ion interface, where the contribution brought by the residual corrosion process is indicated through the impedance  $Z_2$ . This, the impedance is dependent on the frequency.

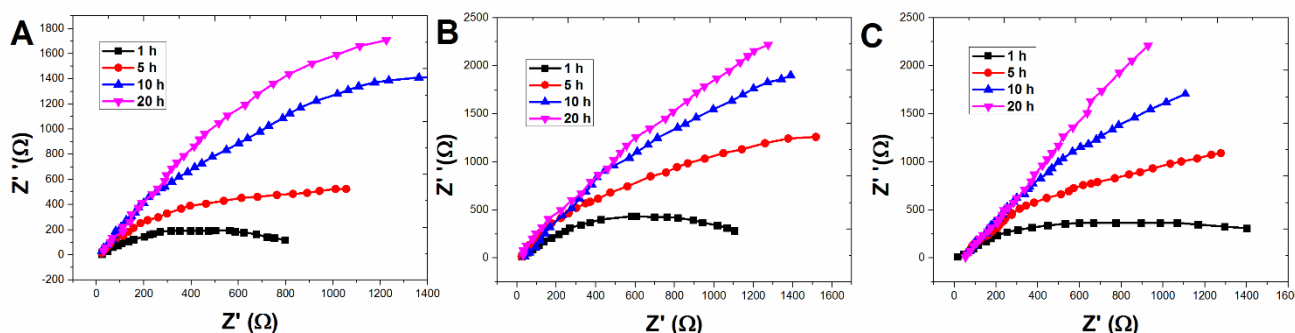


**Figure 2.** Nyquist plots in low-frequency domain. (A) C-1, (B) C-2 and (C) C-3. Initial frequency: 50 KHz; Final frequency: 10 mHz. Amplitude 5 mV.

The Nyquist diagrams in Figure 2A-C exhibit the impedance response measured at diverse times for three samples, with similar variations. The relationship of the time and their  $R_p$  development is indicated in Figure 3. Herein, the low-frequency impedance response reveals  $R_p$ . The three samples share another similarity in the tendency of a primary increase, rapid responses, and a final decline process. In some cases, the formation of a third arc was observed, making the interpretation of the results more complex and raising doubts about the associated phenomena [32]. This is likely to occur in the initial hours of the test later conducted in a passive domain, as the applied electric field and the high alkalinity at the steel surface lead to the polarization of the reinforcing steel. This strengthens the passive film reinforcement as well as continues to protect the steel from being corroded. The impedance response is quite sensitive to the microstructure traits of the cement-based material, as

emphasized by the  $R_p$  variations with time. Herein, the time needed for the activation of the  $R_p$  decrease and the eventual initiation of the corrosion process are significantly impacted by any variation of these traits. This modifies the electrochemical processes at the reinforcing steel surface (anodic oxidation of steel with oxygen reduction) and causes the drop in the  $R_p$  value. Again, it seems that the applied electrical field leads to an acceleration of the corrosion development, allowing better observation of the corrosion initiation [33, 34].

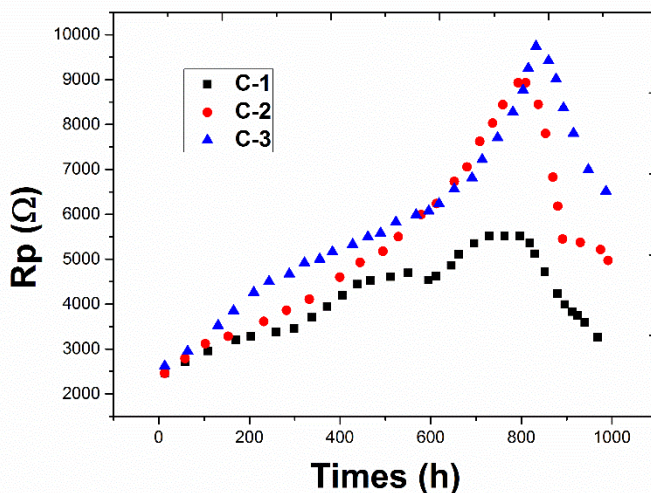


Figure 3. Relationship between polarization resistance values and exposure time of C-1, C-2 and C-3.

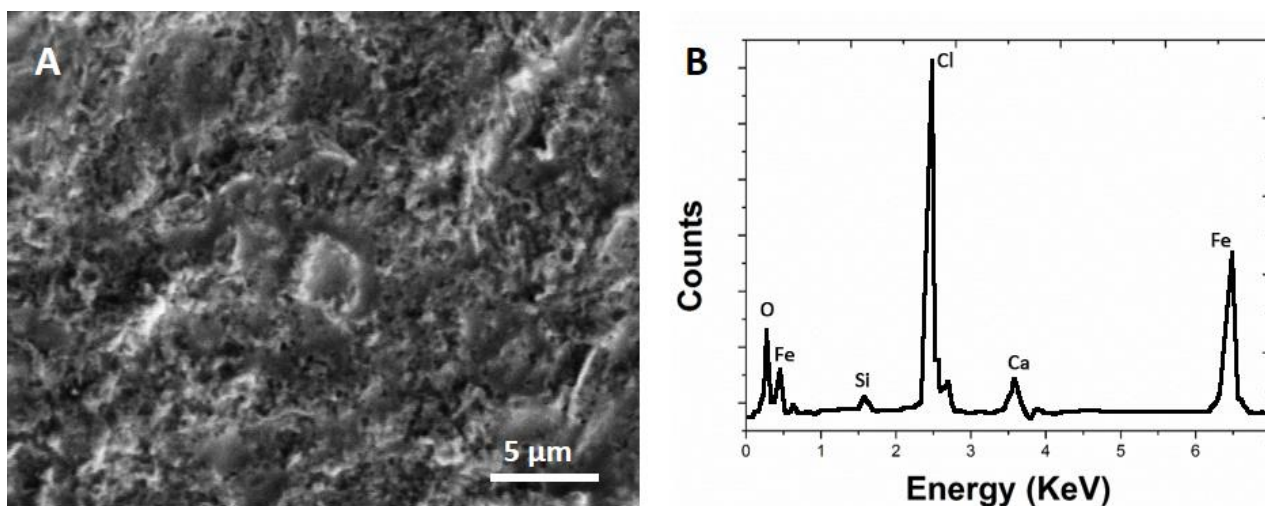
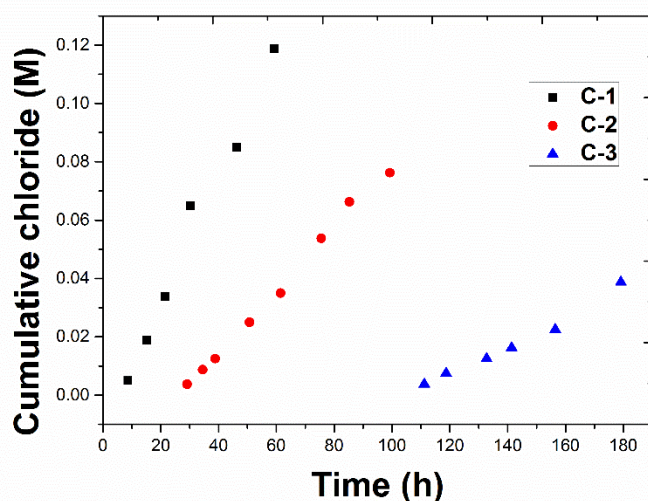


Figure 4. (A) SEM characterization of specimen surface. (B) EDX analysis of the crystals observed.

The  $R_p$  development with time indicates that the reinforcing steel corrosion rate is retarded by this adjoining surface film. In the primary stage, the characterization of the passive layer reinforcement is achieved by the rise in  $R_p$ . After a certain period of time, the thermodynamic stabilization of the

system is achieved, and a plateau of  $R_p$  is obtained with the establishment of the collaborative protection: polarization & alkalinity. The migration of the cement-based material and chlorides occurred during the rise and plateau mentioned above. Pitting corrosion is initiated when the passive film is broken as chlorides in a critical amount arrive at the surface of the reinforcing steel. When they reach the reinforcing steel surface in a sufficient quantity, they break the passive film, and corrosion by pitting starts [35]. This suggests that the applied electrical field leads to an acceleration of the corrosion development, allowing better observation of the corrosion initiation. Herein,  $R_p$  declines in value, suggesting that the electrochemical processes of the steel anodic oxidation via oxygen reduction are modified on the surface of the reinforcing steel. The activation of corrosion can be more favorably observed when the corrosion evolution is accelerated, possibly by the use of an applied electrical field.

Other C-2 samples were further analyzed using a similar impedance procedure. Just as  $R_p$  began to decline in value, the passive state of the steel electrode surface was controlled through the inspection of the EDX analysis and SEM, with data shown in Figure 4B and Figure 4A, respectively, of the destruction of the cement coating. The activation of the corrosion may be directly visually observed. Since no identical mechanisms have been exerted on the entire surface of the reinforcing steel, a heterogeneous surface can be detected. A region with no corrosion products and a domain suggesting pitting corrosion are two conspicuous districts on the surface. The  $R_p$  variations over time highlight the high sensitivity of the impedance response to the microstructural properties of the cement-based material: any variation of these properties has a great influence on the time required to initiate the  $R_p$  drop and consequently to activate the corrosion process. The differences between the thicknesses also explain the localized nature of the corrosion, which occurs at the reinforcing steel surface [36]. The previous region with ample calcium takes the role of the passive layer to defend the steel surface against corrosion. Hence, there are other alternatives to chlorides that can initiate the process of corrosion.



**Figure 5.** Cumulative chloride concentration in the downstream compartment for the C-1, C-2 and C-3.

The threshold value for the concentration of chloride accumulated on the surface of the reinforcing steel is related to the incubation period, but no consensus has been reached on the exact

amount needed to depassivate the surface of the reinforcing steel. To quantify the essential chloride threshold, a first approach is suggested to be an embodied methodology on the basis of Fick's second law, for which information on the diffusion coefficient of the cement-based material is needed.

A classical electrodiffusion cell was employed for obtaining the diffusion coefficient. The application of a constant electric field through the cement-based material sample was achieved by a potentiostat. The potential exerted on the faces of the sample was controlled by a four-point configuration composed of double reference electrodes and a double platinum mesh. A simulated pore solution including KOH (0.083 M) and NaOH (0.025) is present in the downstream compartment, while the upstream compartment is filled with a similar solution containing NaCl (0.5 M), with a known concentration of chloride. After the NaCl is added, potentiometric titration tests were conducted in the presence of silver nitrate in the downstream compartment. The relationship between the time and the cumulative concentration of chloride in the downstream compartment for every ratio of water-cement is shown in Figure 5. As the ratio increases, the diffusion coefficient rises, which highlights that one possibly significant factor that influences the critical threshold level and eventually the structure's service life is the quality of the steel coating. Similar results have been found by other scientists [37]. Under the mortar sample pressure, a range of 0.28 to 1.8 mol/l was observed for the critical chloride concentration in pore solution, with ratios (w/c) ranging from 0.75 to 0.3, as reported by Pettersson [38]. There are two causes of this performance. First, the chloride-binding capacity has been modified. Additionally, as the ratio (w/c) rises, dilution occurs, and the pH value of the concrete pore solution declines. It has been widely recognized that as there is no calcium hydroxide in the voids at the interface, they exert a great impact on the critical threshold level, as a local pH decrease would be resisted by the presence of calcium hydroxide in these areas [39].

#### 4. CONCLUSIONS

An effective method was proposed in this work to determine the critical concentration threshold value for the initiation of reinforcing steel (embedded in a cement-based material sample) corrosion. The correlation of the corrosion initiation and impedance response is emphasized by a comparison of the results. The activation of the chloride corrosion is associated with a significant impedance response decline in the capacitive part, as indicated by multielementary analyses, SEM observations and the "low-frequency" impedance response.

#### References

1. M. Mazloom, A. Ramezaniapour and J. Brooks, *Cement and Concrete Composites*, 26 (2004) 347.
2. O. Poupard, A. Aït-Mokhtar and P. Dumargue, *Cement and Concrete Research*, 34 (2004) 991.
3. A. Tarighat and B. Zehtab, *Arabian Journal for Science & Engineering*, 41 (2016) 1.
4. L. Wu, X. Kou and M. Jiang, *Arabian Journal for Science & Engineering*, 40 (2015) 1.
5. L. Wang, C. Li and J. Yi, *Journal of Coastal Research*, 73 (2015) 259.
6. F.L. Fei, J. Hu, Q.J. Yu, J.X. Wei and Y.B. Nong, *Materials & Corrosion*, 66 (2015) 1039.
7. J.H. Li, B. Zhao, J. Hu, H. Zhang, S.G. Dong, R.G. Du and C.J. Lin, *Int. J. Electrochem. Sc.*, 10

- (2015) 956.
8. C. Sun, S. Liu, J. Niu and W. Xu, *Int. J. Electrochem. Sc.*, 10 (2015) 5309.
  9. J. Hu, X. Cheng, X. Li, P. Deng and G. Wang, *Journal of Chemistry*, 2015 (2015) 1.
  10. T. El-Maaddawy, A. Bouchair, A.S. El-Dieb and A. Biddah, *Journal of Composites for Construction*, 19 (2015) 12.
  11. S. Park, S. Ahmad, C.-B. Yun and Y. Roh, *Experimental Mechanics*, 46 (2006) 609.
  12. J.-W. Kim, C. Lee, S. Park and K.-T. Koh, *KSCE Journal of Civil Engineering*, 17 (2013) 1432.
  13. D. Ribeiro and J. Abrantes, *Construction and Building Materials*, 111 (2016) 98.
  14. Y. Liang, D. Li, S.M. Parvasi, Q. Kong and G. Song, *Smart Materials and Structures*, 25 (2016) 095003.
  15. A. Narayanan and K.V. Subramaniam, *Smart Materials and Structures*, 25 (2016) 095011.
  16. X. Zhao and J. Xiong, *Int. J. Electrochem. Sc.*, 11 (2016) 5702.
  17. F. Guo, Z. Yu, P. Liu and Z. Shan, *Research in Nondestructive Evaluation*, 27 (2016) 26.
  18. M. Lunak, I. Kusak and D. Stefkova, *Procedia Engineering*, 151 (2016) 265.
  19. J. Deus, B. Díaz, L. Freire and X. Nóvoa, *Electrochimica Acta*, 131 (2014) 106.
  20. V. Talakokula, S. Bhalla and A. Gupta, *Journal of Intelligent Material Systems and Structures*, 25 (2014) 484.
  21. A. Narayanan and K.V. Subramaniam, *Construction and Building Materials*, 105 (2016) 536.
  22. B. Dong, Y. Wang, W. Ding, S. Li, N. Han, F. Xing and Y. Lu, *Construction and Building Materials*, 56 (2014) 1.
  23. X. Hu, H. Zhu and D. Wang, *Sensors*, 14 (2014) 19897.
  24. C. Alexis, B. Franck, D. Didier, A. Emmanuel and C. Hangseok, *Composites Part B: Engineering*, 69 (2015) 350.
  25. K.K. Sago-Crentsil, F.P. Glasser and J.T.S. Irvine, *British Corrosion Journal*, 27 (1992) 113.
  26. D.G. John, P.C. Searson and J.L. Dawson, *British Corrosion Journal*, 16 (1981) 102.
  27. L. Hachani, J. Carpio, C. Fiaud, A. Raharinaivo and E. Triki, *Cement & Concrete Research*, 22 (1992) 56.
  28. K.K. Sago-Crentsil, F.P. Glasser and J.T.S. Irvine, *British Corrosion Journal*, 27 (1991) 113.
  29. L. Lemoine, F. Wenger and J. Galland, *Astm Special Technical Publication*, (1990) 118.
  30. D.G. John, P.C. Searson and J.L. Dawson, *British Corrosion Journal*, 16 (1980) 102.
  31. C. Andrade, I.R. Maribona, S. Feliu, J.A. González and S.F. Jr, *Corrosion Science*, 33 (1992) 237.
  32. D. Ribeiro, C. Rovere, C. Souza, S. Kuri, J. Labrincha, J. Abrantes and M. Morelli, *ISRN Materials Science*, 2011 (2011)
  33. M. Criado, I. Sobrados, J.M. Bastidas and J. Sanz, *Progress in Organic Coatings*, 88 (2015) 228.
  34. M. Chevalier, F. Robert, N. Amusant, M. Traisnel, C. Roos and M. Lebrini, *Electrochimica Acta*, 131 (2014) 96.
  35. O. Poupard, A. Aıt-Mokhtar and P. Dumargue, *Cement and Concrete Research*, 34 (2004) 991.
  36. R. Nagalakshmi, L. Nagarajan, R.J. Rathish, S.S. Prabha, N. Vijaya, J. Jeyasundari and S. Rajendran, *Int. J. Nano. Corr. Sci. Engg.*, 1 (2014) 39.
  37. G.K. Glass, N.M. Hassanein and N.R. Buenfeld, *Magazine of Concrete Research*, 49 (1997) 323.
  38. K. Pettersson, *Cbi Report*, 20 (1992) 461.
  39. G.K. Glass and N.R. Buenfeld, *Corrosion Science*, 39 (1997) 1001.